

CRACKING RISK OF THE CONCRETE CRUST OF A NUCLEAR POWER STATION

By

GY. BALÁZS—J. FEHÉR—A. TÓTH—I. ZSIGOVICS

Department of Building Materials, Technical University, Budapest

Received: March 16, 1981

Concrete structure of the *Paks Nuclear Power Station* has large dimensions hence a huge mass, subject to crustal and running cracks in the days after concreting if combined inherent and working load stresses exhaust concrete ultimate strain. Inherent stresses may result from the inhomogeneities in temperature distribution and uneven shrinkage in the concrete because in these cases the pertaining deformations are inhibited.

Our research work omitted concrete shrinkage stresses, the shuttering having been made of plywood 15 or 30 mm thick, preventing water losses hence counteracting any important shrinkage until stripping. In the following, only inherent stresses due to heat gradients will be concerned with.

Temperature has a complex effect. Temperature developing in the concrete depends on the concrete temperature at concreting, on the subsequent air temperature, on the cement hydration heat, on the sunshine, evaporation, on the dimensions and thermal characteristics of the r.c. wall, and on the shuttering features.

From the aspect of concrete thermal stresses, the increase of concrete tensile strength and modulus of elasticity with age has to be reckoned with. Besides, since inherent stresses are other than instantaneous, also creep arises, of a value varying with time.

Thus, stress state of mass concrete is a complex problem. Practical design methods involve rather rough approximations of the effect of several factors on thermal stresses, in particular in green concrete, and of the importance of their history. These approximations can be motivated by the variation with time of the modulus of elasticity and of the creep rate.

Neither could we ourselves undertake else than approximate calculations. To reduce the sources of error, the problem has been solved in several steps (the mechanical characteristics of concrete were not integrated into the computer program) for a better checking of partial results. Thereby e.g. the temperature calculation seems to be rather reliable by being checked on a full-scale model.

Our calculations on the effect of each factor usually omitted the creep effect. Creep reduces the stress, as it will be outlined below.

1. Computer program for the calculation of temperature gradient across the concrete cross section

1.1 Theoretical bases of the calculation of two-dimensional, unsteady-state temperature field

One dimension of the tested block much exceeding both others, the two-dimensional temperature distribution along the cross section has only been examined. Under the given conditions not even this problem reduced to a plane could be solved analytically, forcing us to apply an approximate solution easy to be programmed for a computer. The computer program relied on the following model:

Unsteady-state temperature gradient across a solid including inner heat sources is known to be obtained by solving a differential equation for heat conduction containing the source term [1]. In the actual case, the problem is a two-dimensional one, leading to the equation:

$$c \cdot \rho \frac{\partial t(x, y, \tau)}{\partial \tau} = \left(\frac{\partial}{\partial x} + \frac{\partial}{\partial y} \right) [\lambda \cdot \text{grad } t(x, y, \tau)] + \dot{q}$$

where c , ρ and λ are specific heat, mass density and thermal conductivity of the given material, respectively, $t(x, y, z, \tau)$ is the temperature at a point with coordinates x, y, z of the solid at time τ , and \dot{q} is the heat developing (or vanishing) in unit volume of a given spot of the solid, during unit time.

In general \dot{q} , c and λ may be space and time-dependent magnitudes, while boundary conditions are partly of the first kind (the soil at a given depth being at a given temperature), and partly, of the third kind (air temperature being given). A usual method of solution of the differential equation above is the so-called method of finite differences where the differential equation is transformed to finite difference equations for consecutive small time intervals $\Delta\tau$ and elementary volumes ΔV , yielding elementary volume temperatures at any time interval $\Delta\tau$ as solutions of a linear algebraic equation system. At a difference from several published methods of establishing difference equation systems (e.g. [2]), in the actual case the mathematically equivalent method of elementary heat balance equations has been applied [3], leading to a system of equations essentially identical to the one obtained by the method of finite differences such as:

Let us take an elementary volume ΔV_i around a point of the considered solid, receiving heat from, and emitting to, adjacent elementary volumes. Be these — positive or negative — heat flows affected by a sign: $I_1^i(\tau)$, $I_2^i(\tau)$, $I_3^i(\tau)$, . . . $I_n^i(\tau)$ at a time τ ; $\dot{q}_i(\tau)$ the heat developing in unit volume during unit time; ρ_i the mass density at the given spot; c_i its specific heat; and $t_i(\tau)$

the temperature of the elementary volume; then the heat accumulated in the elementary volume during time $\Delta\tau$ within the time interval $(\tau, \tau + \Delta\tau)$:

$$\begin{aligned}\Delta Q^i &= [I_1^i(\tau) + I_2^i(\tau) + \dots + I_n^i(\tau) + \dot{q}_i(\tau) \cdot \Delta V_i] \cdot \Delta\tau = \\ &= \left[\sum_{j=1}^n I_j^i(\tau) + \dot{q}_i(\tau) \cdot \Delta V_i \right] \cdot \Delta\tau.\end{aligned}$$

Its effect is to change the temperature of the elementary volume to some value $t_i(\tau + \Delta\tau)$ known to be related to the absorbed heat as:

$$\Delta Q^i = c_i \cdot \rho_i \cdot \Delta V_i \cdot [t_i(\tau + \Delta\tau) - t_i(\tau)].$$

Substituting the heat value in terms of flows and sources yields for the changed temperature of the i -th elementary volume:

$$t_i(\tau + \Delta\tau) = t_i(\tau) + \frac{\Delta\tau}{c_i \rho_i \Delta V_i} \left\{ \sum_{j=1}^n I_j^i(\tau) + \dot{q}_i(\tau) \cdot \Delta V_i \right\}$$

$i = 1, 2, 3 \dots N$ (N being the total number of elementary volumes).

In knowledge of initial temperatures of each elementary volume, sources \dot{q}_i and flows I_j^i , time variation of the temperature in each elementary volume can be computed.

Remind that this method is only applicable in knowledge of heat flows I_j^i and heat sources \dot{q}_i . Let us outline now the types of heat flow and heat source encountered in the examined cases, and the way how they were taken into account.

a) *Heat conduction*

In the inner parts of the tested solid, heat is transferred by conduction described by the known law:

$$I_{\text{cond}} = \frac{\lambda}{d} \cdot (t_2 - t_1) \cdot \Delta A$$

where λ is a generally place and time-dependent coefficient of heat conductivity, d is the spacing between spots at temperatures t_1 and t_2 , and ΔA is a surface normal to the heat flow.

b) *Heat exchange by convection*

For solid/air interfaces, the known law of heat transfer

$$I_{\text{conv}} = \alpha \cdot (t_f - t_k) \cdot \Delta A$$

has been applied, where α is the so-called heat transfer coefficient, t_f the surface temperature, and t_k the ambient temperature. The heat transfer coefficient has been expressed by taking the wind effect into consideration [4]:

$$\alpha(t, v) = 7.32 \cdot v^{0.656} + B \cdot |t_f - t_k|^{1/3} \cdot e^{-1.9 \cdot v}$$

where v is the wind velocity and B a constant depending on the surface position.

c) Heat exchange by thermal radiation

Interfaces with air are affected by another heat flow resulting from the radiational interaction with surrounding objects and with the atmosphere, expressed by [3]:

$$I_{\text{rad}} = 5.7 \cdot a_f \cdot \left\{ \left(\frac{t_s + 273}{100} \right)^4 - \left(\frac{t_f + 273}{100} \right)^4 \right\} \cdot \Delta A.$$

Here a_f is the surface blackness degree, and t_s the temperature of the material irradiating the surface in question, a value depending on the vapour pressure and the ambient temperature t_k if there is an interaction with the atmosphere [5].

d) Insolation

Temperature development is also affected by insolation, to be considered as a source on insolated surface parts. For an insolation intensity I_N and an insolation absorption coefficient A_N of the surface, the source is expressed by:

$$\dot{q}_N = A_N \cdot I_N \cdot \frac{\Delta A}{\Delta V}.$$

(ΔV being the size of the considered volume element); I_N may of course vary with time.

e) Heat of cement hydration

Also hydration heat may be reckoned with as a heat source variable with time:

$$\dot{q}_B = \dot{q}_B(\tau).$$

Function $\dot{q}_B(\tau)$ has been determined experimentally for each cement type concerned.

1.2 Basic data used in computation

The first computation was made under conditions of the model test [6] in autumn 1977 as a comparison between calculated and experimental results.

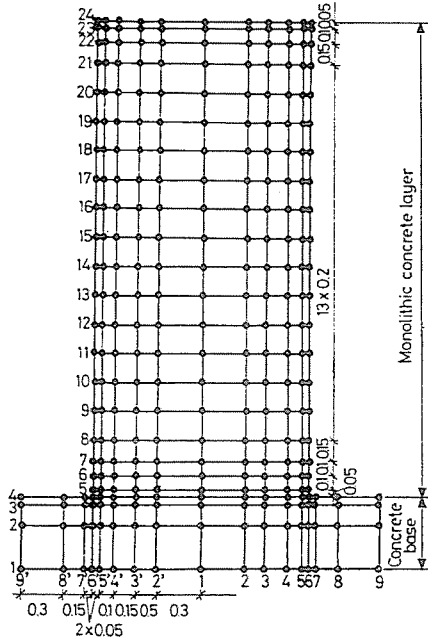


Fig. 1. Network on a continuously concreted mass

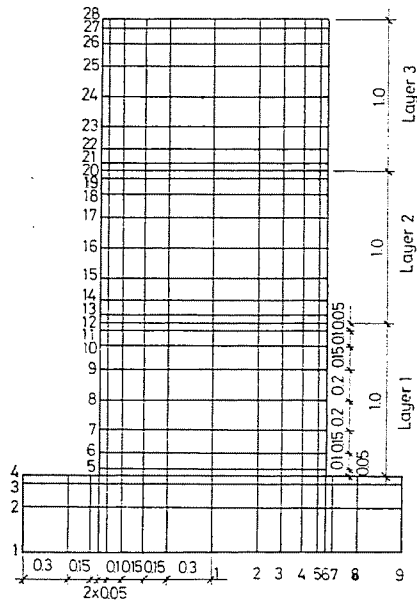


Fig. 2. Network on a section-wise concreted mass

Figures 1 and 2 represent the networks for monolithic and section-wise concreted blocks in the nodes of which the temperatures depending on time have been computed.

In checking the computer analysis by means of model tests, from among weathering conditions the air temperature values relied on field measurements [6] compared with data supplied by the Meteorological Station. Insolation intensity values could not be measured neither acquired from the Meteorological Station. Wind velocity was assumed at an average of 2 m/sec, based on data delivered by the Meteorological Station.

Comparative calculations involved data in Table 1. Three different hydration heats were assumed — under adiabatic conditions — corresponding to summer air temperature, moderate spring and autumn temperatures and summer temperature with setting retarder (Fig. 3). Both insolation intensity (Fig. 4) and air temperature (Fig. 5) were taken from records of the Meteorological Station, again corresponding to summer, spring and autumn values.

Thermal conductivity of the shuttering was determined in a *Bock* equipment. Solid density of 15 mm and 30 mm plywood is 680 kg/m^3 , its dry thermal conductivity is 0.11 W/mK , its specific heat being 2.51 kJ/kgK , according to published data. Thermal conductivity coefficient of the plastic foam of an assumed solid density of 30 kg/m^3 is 0.05 W/mK .

Although the thermal conductivity of green concrete has also been determined conventionally, in a *Bock* equipment in steady heat flow, but it was not reassuring. Namely the test lasted some hours meanwhile the thermal condition of concrete changed because of the hydration heat development, and also vapour migration started, affecting measurement results. Therefore

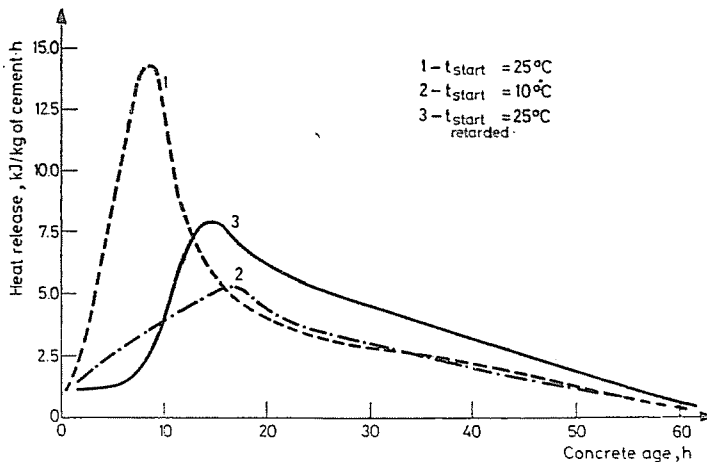


Fig. 3. Hydration heat functions assumed in computation (fly-ash portland cement 350 ppc 10 from Beremend)

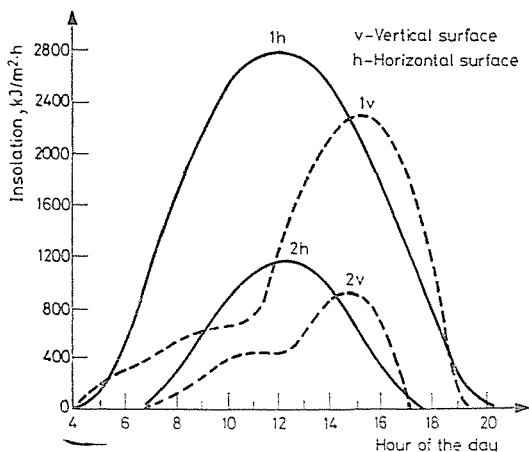


Fig. 4. Sunshine intensity

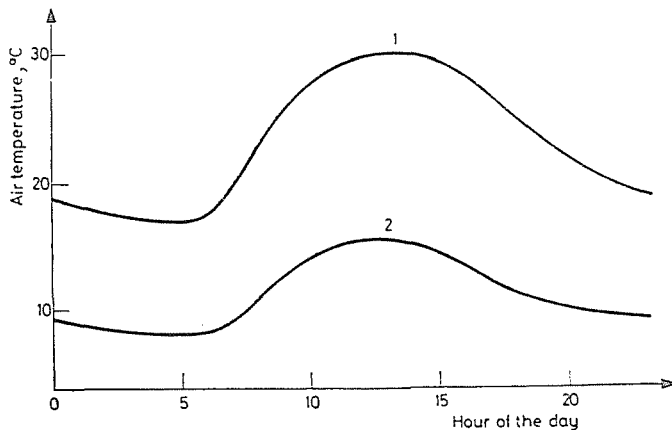


Fig. 5. Air temperature vs. time

an unsteady-state measurement method lasting 30 sec was applied. Thermal conductivity coefficients determined by both methods are rather different. Measurements in unsteady heat flow in the first 30 to 50 hours gave 3.2 to 3.5 W/mK for a concrete of 2100 kg/m^3 solid density, and 5.5 to 6.3 W/mK for a heavy concrete of 3960 kg/m^3 density (with hematite and steel balls as aggregate). Similar thermal conductivities have been recorded in erected dams, and a confrontation with model test results shows these values to be acceptable.

In conformity with published data, the specific heat of silica gravel concrete of 2100 kg/m^3 solid density was assumed at 0.88 kJ/kgK , and of hematite concrete of 3960 kg/m^3 solid density at 0.69 kJ/kgK .

Also from published data and our experimental results, the thermal expansion coefficient of concrete was assumed

for concrete of 2100 kg/m^3 solid density at $10 \cdot 10^{-6}/^\circ\text{C}$

for heavy concrete at $11 \cdot 10^{-6}/^\circ\text{C}$.

2. Effect of different factors on crustal cracking

Computer analysis was only concerned with temperature gradients, to be considered as reliable, since the material characteristics used in computer calculations were checked by model tests. Thereafter thermal stresses were determined from temperature gradients as follows:

- Thermal stresses (inherent stresses) were assumed according to Fig. 6.
- Plotting the mean temperature in the region exposed to tensile stress vs. time (e.g. Fig. 7), the mean temperature $\bar{\tau}$ at the tested age was determined by planimetry.

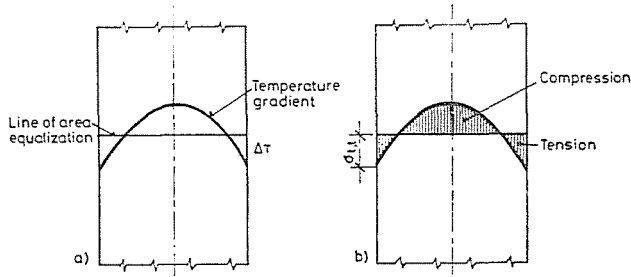


Fig. 6. Stresses due to uneven heat distribution

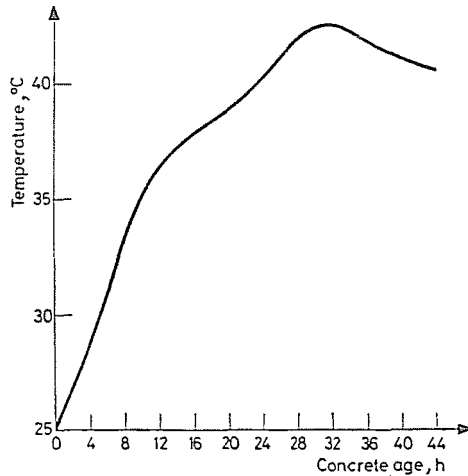


Fig. 7. Mean temperature distribution vs. concrete age in the tensile zone according to Fig. 6 for example 1

- Using the mean temperature, formula $t_{20} = \frac{\bar{\tau} + 10}{30} t$ was applied to calculate the equivalent concrete age (t being the real concrete age), assuming the concrete strength and modulus of elasticity at a given age and temperature to become as high as at 20 °C at the equivalent age t_{20} .
- The time behaviour of the concrete modulus of elasticity in compression (Fig. 8), prism strength $R_{c,pr}$ and solid strength R_c at 20 °C (Fig. 9) were experimentally determined.
- Also the time variation of the bending-tensile strength $R_{t,j}$ of concrete was measured. The result, together with earlier test results, was applied to calculate the pure tensile strength $R_{t,t}$.
- The equivalent age was applied to determine the modulus of elasticity of concrete from Fig. 8, the tensile strength from Fig. 9.
- The $\sigma_{t,t_{max}}$ value was calculated from the formula

$$\sigma_{t,t_{max}} = \alpha \cdot E_0 \cdot \Delta\tau$$

assuming identity of moduli of elasticity in tension and in compression, and the concrete to be in the elastic range.

- Cracking is not imminent for $\sigma_{t,t_{max}} < R_{t,t}$.

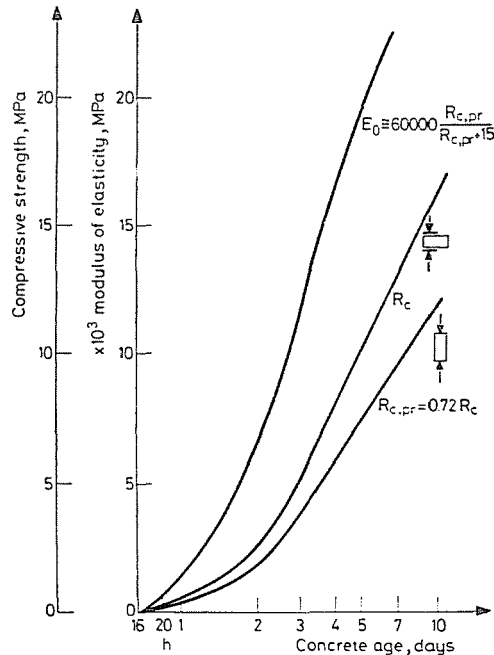


Fig. 8. Experimental basic curves (compressive strength, modulus of elasticity, retarded setting) assumed in the computation

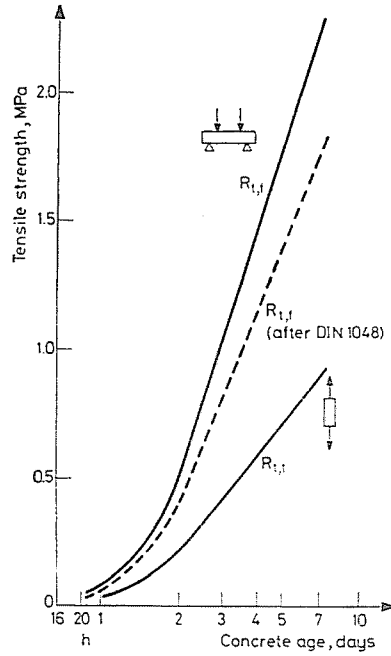


Fig. 9. Basic curve of tensile strength $R_{t,t}$ assumed in the computation, calculated from experimental bending-tensile strength data

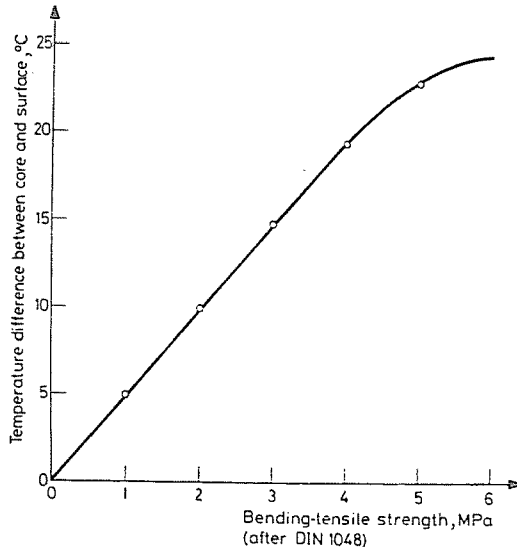


Fig. 10. Risk of cracking according to DIN 1048

- The risk of cracking was also checked according to the RILEM directives. Accordingly, there is no risk of cracking if the bending-tensile strength $R_{t,t}$, determined from Fig. 7 according to DIN 1048 exceeds the bending-tensile strength determined from Fig. 10 on the basis of the maximum temperature difference.
- At last, stress reduction due to creep was examined.

To examine the effect of each factor, examples tabulated in Table 1 were solved. In the following, the effect of creep to reduce the stresses will be omitted, biasing the stress values but safeguarding the ratio of stresses.

Table 1
Computer inputs (assumptions)

Example No.	Concrete grade	Hydr. heat*	Shuttering	Air temp.** Insolation***	Wind velocity km/h	Concreting	Running time, concreting time
1	2	3	4	5	6	7	8
1	B 200	1	15 mm plywood	1	60	Continuous	3 days, 12 h, $\lambda = 4.64$
2	B 200	1	15 mm plywood	1	60		
3	B 200	1	30 mm plywood	1	60		
4	B 200	1	15 mm plywood	1	0		
5	B 200	3	15 mm plywood	1	60		
6	B 200	3	15 mm plywood + 20 mm plastic foam	1	60		
7	B 200	2	15 mm plywood	2	60		
8	B 200	2	15 mm plywood + 20 mm plastic foam	2	60		
9	B 200	2	15 mm plywood	1	60	intermittent	
10	B 200	3	15 mm plywood	1	60		
11	B 200	1	15 mm plywood	1	60	Continuous	3 days, 12 h, $\lambda = 8.1$
12	B 200	1	30 mm plywood	1	60		3 days, 12 h, $\lambda = 8.1$
13	B 200	1	15 mm plywood + 20 mm plastic foam	1	60		7 days + 1 day strip-ped, 12 h, $\lambda = 8.1$
14	B 200	1	15 mm plywood + 20 mm plastic foam	1	60		3 days + 2 days strip-ped, 12 h, $\lambda = 8.1$
15	B 200	1	15 mm plywood	1	60		3 days, 6 h, $\lambda = 8.1$
16	B 200	1	15 mm plywood	3+1	60		3 days, 12 h, $\lambda = 8.1$
17	B 200	1	15 mm plywood	1	60		3 days, 12 h, $\lambda = 4.64$
18	B 200	1	15 mm plywood	1	60		3 days, 12 h, $\lambda = 2.32$

* Denoted according to Fig. 3
 ** Denoted according to Fig. 5
 *** Denoted according to Fig. 4

a) Effect of the shuttering

Thermal insulation of the shuttering much affects thermal conditions within the wall. The controlling effect of shuttering clearly appears from Table 2 referring to an assumed summer air temperature and a wind velocity of 60 km/h.

Table 2
The effect of shuttering on thermal stresses

Example No.	Shuttering	Concrete age, hours	$\sigma_{t,t_{max}}$ MPa	$R_{t,t}$ MPa	Ratio
11	15 mm plywood	20	0.41	0.23	1.78
11	15 mm plywood	44	1.02	0.57	1.79
12	30 mm plywood	20	0.26	0.23	1.13
12	30 mm plywood	44	0.65	0.58	1.12
13	15 mm plywood + 20 mm plastic foam	20	0.13	0.23	0.57
13	15 mm plywood + 20 mm plastic foam	44	0.30	0.59	0.51
1	15 mm plywood	44	1.24	0.57	2.18
3	30 mm plywood	44	0.83	0.57	1.46
5	15 mm plywood	44	0.68	0.36	1.89
6	15 mm plywood + 20 mm plastic foam	44	0.25	0.38	0.68
7	15 mm plywood	44	0.58	0.34	1.71
8	15 mm plywood + 20 mm plastic foam	44	0.18	0.35	0.51

The effect of shuttering on the temperature gradient has also been plotted in Fig. 11. Increasing the shutterboard thickness from 15 to 30 mm reduced the $\sigma_{t,t_{max}}/R_{t,t}$ ratio to 0.63. Lining the 15 mm plywood shuttering by 20 mm plastic foam reduced the ratio to 0.32 (as seen from examples 11 to 13).

To evaluate, however, the effect of shuttering, also the age at stripping has to be taken into consideration. The case of 15 mm plywood + 20 mm plastic foam (examples 13 and 14) yielded values seen in Table 3.

Table 3
The effect of stripping time on thermal stresses

Example No.	Stripping time h	Concrete age days	$\sigma_{t,t_{max}}$ MPa	$R_{t,t}$ MPa	Ratio
13	168	184	2.34	1.39	1.68
14	72	84	3.03	0.96	3.16

The risk of cracking is much higher for stripping at 72 hours than at 7 days of age (Fig. 12). Namely, while at 3 days the max. temperature of concrete just starts decreasing compared to the absolute maximum, at 7 days of age the temperature of concrete has already dropped from the maximum of 49 °C to 35 °C. Meanwhile the concrete tensile strength grew from 0.96 to 1.39 MN/m². In our example, the risk of cracking was about halved by concret-

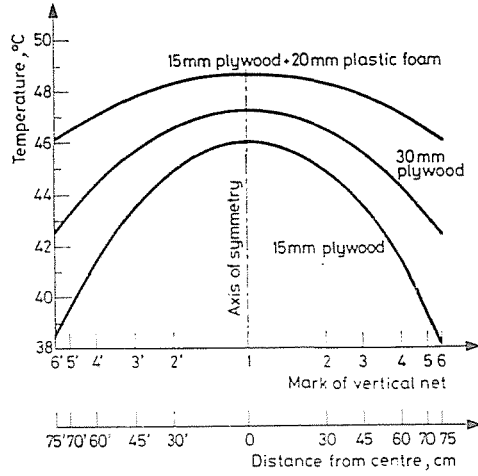


Fig. 11. Effect of shuttering on temperature distribution

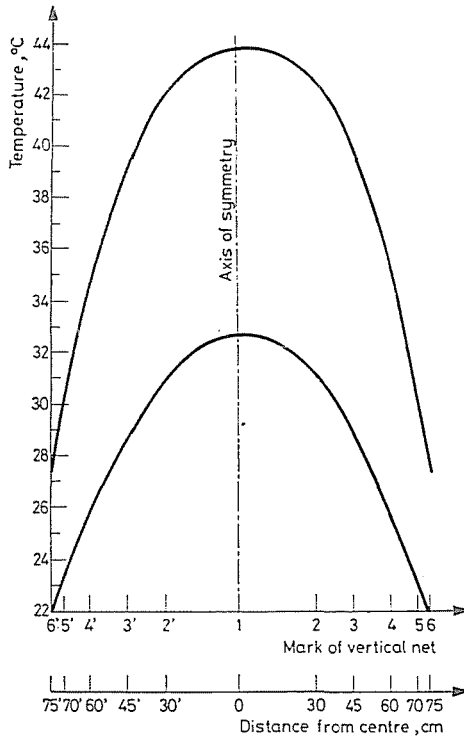


Fig. 12. Effect of stripping time on temperature distribution

ing in hot weather and stripping at 7 rather than at 3 days of age. It would be further reduced by removing first the plastic foam lining rather than both layers at once.

b) *Concrete strength*

Laboratory tests showed the rate of hardening of concretes of two different mass densities but otherwise identical qualities (about the same cement type, consistence, etc.) to be about the same. Thus, moduli of elasticity and tensile strengths of concretes of the same age, cured under identical conditions, were considered as equal.

c) *Intermittent concreting*

Intermittent concreting was assumed to be made in 1.5 m thick layers. Concreting intermittently rather than continuously reduces the thermal stress maxima 48 hours after the first concreting to about 2/3, and for concreting every second day, to about the half. Thus, intermittent concreting essentially controls the temperature.

Comparison of stress conditions in examples 5 and 10 at 48 hours of age:

	$\sigma_{t,t_{\max}}$ MPa	$R_{t,t}$ MPa	Ratio r
Example 5	0.68	0.36	1.88
Example 10	0.38	0.34	1.11

These examples started from the worst case. For a lower temperature at concreting, thermal stresses are less severe. A setting retarder does not influence the total heat released but reduces the initial heat release. Comparison of examples 5 and 10 shows that in case of retarded hardening, assuming continuous concreting, at 44 hours of age, $r = 1.88$, changing to 1.11 for section-wise concreting with 1 day of intermittence. Thus, also admixture of a setting retarder acts favourably.

d) *Wind effect*

Comparison of examples 1 and 4 shows the wind to have a marked effect on the time behaviour of temperature. In case of a wind velocity of 60 km/h near the exposed concrete surface, the surface temperature fluctuated about a constant value, corresponding to air temperature and insolation (Fig. 13).

Table 4
Stresses due to uneven temperature distribution.
Example 10
 (Sections concreted at daily intervals)

Horizontal plane (Fig. 2)	Concrete age days	Δt °C	Equivalent age h	$E_{o,c}$ MPa	$\sigma_{t,tmax}$ MPa	$R_{t,t}$ MPa
8	8	0.60	9.78	—	—	—
	12	1.30	15.02	—	—	—
	16	2.80	20.36	500	0.014	0.020
	20	3.60	25.82	800	0.029	0.025
	24	2.00	31.46	3 100	0.062	0.080
	32	1.80	43.11	5 500	0.099	0.170
	40	4.50	55.37	8 400	0.378	0.280
	48	3.50	67.25	11 400	0.399	0.395
	64	4.65	91.82	16 200	0.753	0.560
72	3.00	103.46	17 900	0.537	0.625	
16	8	0.50	9.78	—	—	—
	12	1.70	15.07	—	—	—
	16	3.35	20.58	600	0.020	0.020
	20	4.10	26.45	1 900	0.078	0.045
	24	2.80	32.18	3 300	0.092	0.080
	32	2.50	44.71	5 700	0.143	0.175
	48	4.10	70.50	12 200	0.500	0.420
24	8	0.50	9.87	—	—	—
	12	1.70	15.16	—	—	—
	16	3.40	20.71	600	0.020	0.020
	20	4.30	26.45	1 900	0.082	0.045
	24	3.10	32.45	3 300	0.102	0.080

At calm, however, temperature fluctuation arose about the inner temperature (Fig. 14).

The wind effect is also manifest on shuttered surfaces. Stresses at 44 hours of age:

	$\sigma_{t,tmax}$ MPa	$R_{t,t}$ MPa
Example 1	1.24	0.57
Example 4	0.97	0.60

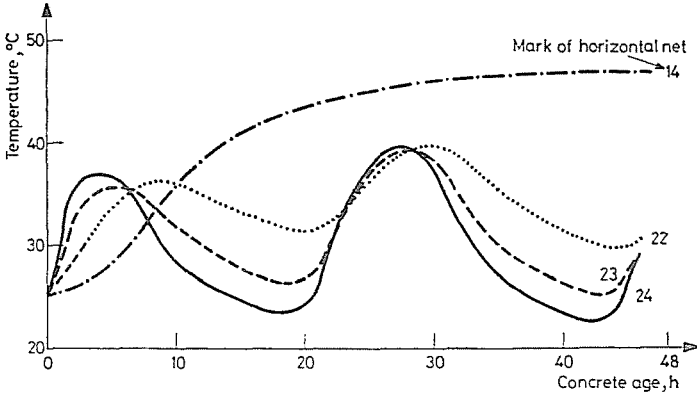


Fig. 13. Timely development of temperature for example 1 (along vertical mid-plane 1 in Fig. 1)

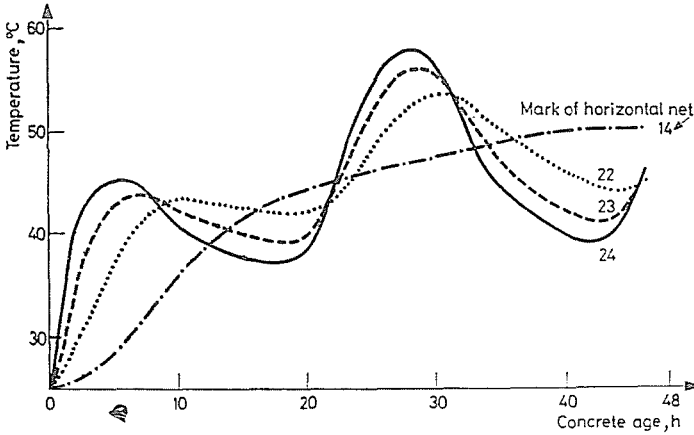


Fig. 14. Timely development of temperature for example 4 (along vertical mid-plane 1 in Fig. 1)

The max. tensile stress in concrete shuttered in 15 mm plywood was 1.24 MN/m² in case of a wind velocity of 60 km/h, it decreased to 0.97 MN/m² at calm.

e) *Effect of insolation and temperature*

Concreting in autumn (concrete at 10 °C) rather than in summer (concrete at 25 °C) reduced the $\sigma_{t,i,max}$ to $R_{t,i}$ ratio to :

	$\sigma_{t,tmax}$ MN/m ²	$R_{t,t}$ MN/m ²	Ratio
Example 1	1.24	0.57	2.18
Example 7	0.53	0.34	1.56

f) *Effect of the thermal conductivity of concrete*

Comparison of examples 11, 17 and 18 permits to conclude on the effect of the variation of thermal conductivity in concrete. Figure 15 and Table 4 show the maximum temperature of concrete to decrease slightly with increasing λ , and so does the developing thermal stress. Namely, Fig. 16 shows the temperature curve shape to change with decreasing λ .

Thermal conductivity is not constant in green concrete. In a concrete of a mass density of 2100 kg/m³ — in unsteady heat flow — $\lambda = 3.2$ to 3.5 W/mK values have been measured, in agreement with mass concrete measurements. The value $\lambda = 4.65$ was assumed in calculation since in this case the measured and the calculated temperatures agreed. The difference is likely to be due to the reinforcement.

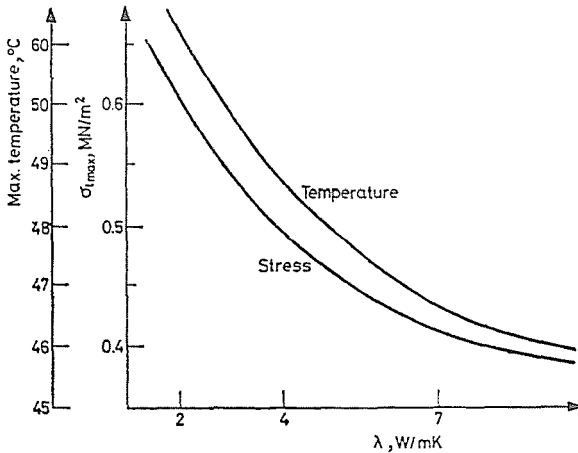


Fig. 15. Effect of λ on thermal stresses

g) *Effect of the cement hydration heat*

The cement type has the greatest effect on thermal stresses (Fig. 17). Our tests have shown the cement 350 ppc 10 from *Beremend* used in the project and in our tests to be a normal portland cement from the aspect of hydration heat, it being 293 J/g for the first 7 days.

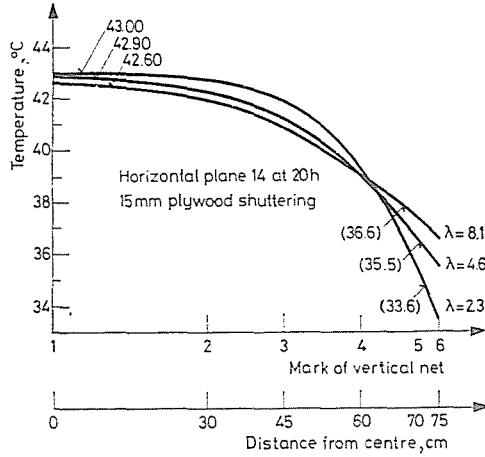


Fig. 16. Effect of λ on temperature distribution

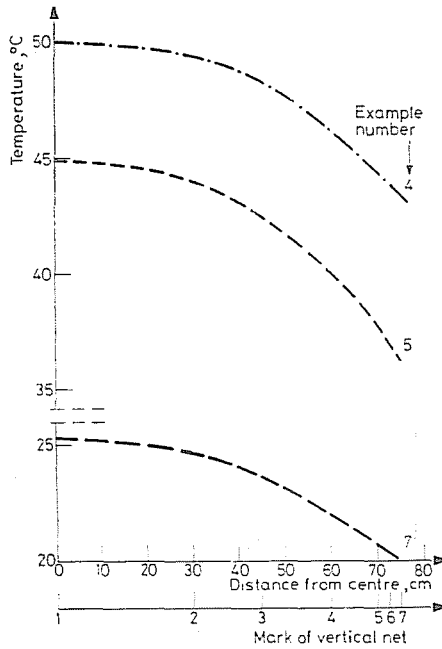


Fig. 17. Horizontal temperature gradient at wall mid-height

3. Observations on crustal cracks

Observation of the reinforced concrete walls of the *Paks Nuclear Power Station* made of a concrete of 2100 kg/m^3 mass density hardly showed crustal cracks (except for exposed concrete surfaces). In most of the presented exam-

ples, extreme climatic conditions have been assumed (summer temperature, intensive insolation, wind velocity of 60 km/h). Also from the aspect of concrete characteristics the worst case was assumed, namely that the concrete behaves elastically. Thus, the real risk of cracking is less than assumed in calculations. Tendencies, however, have been estimated correctly.

What is the explanation that effective thermal stresses are lower than the calculated ones?

A theory has been found in the literature that thermal stresses cause variable permanent loads accompanied by creep, of a value that can at most be assessed. WISCHERS [7] suggested a creep coefficient $\varphi = 1$ for approximate calculations. It would exactly halve the stress as seen from

$$\sigma_{i,t_{\max}} = \alpha \cdot \Delta\tau \cdot \frac{E_0}{1 + \varphi}.$$

Our research work hints to another possibility (without denying the creep) illustrated in Fig. 18. Starting from example 1, temperature gradients at 8, 12 and 44 hours have been plotted. Already at 8 h, the concrete temperature rose compared to the freshly placed one, with little temperature difference across the cross section. But at 12 hours, there is already an important temperature difference that continues to grow. Concrete in setting is still plastic, responding to temperature variation by deforming without stress development. The time in hours when deformations become inhibited could only be determined by deformation measurements within the concrete mass. It seems us that the temperature developing at a given time has to be reduced by that where deformations start to be inhibited. In the presented example (Fig. 18), at 44 hours of age, $\Delta\tau = 5.2$ °C. Subtracting from the temperature diagram at 44 hours that at 8 hours yields $\Delta\tau = 4.9$ °C, hardly any decrease. Subtracting, however, the 12 hours' temperature curve from the 44 hours' one yields $\Delta\tau = 2.7$ °C, an important difference about corresponding to the assumed $\varphi = 1$.

The risk of cracking of concrete of a mass density of 2100 kg/m³ has also been checked according to the RILEM directives. Examples 1 to 4 show the risk of cracking determined by this method to be better by about 25% than the computer output.

This difference may involve the creep effect.

The crack is at most 150 mm deep but generally less (Fig. 19). Both the stress diagram and the crack depth depend on the shape of the temperature distribution, depending primarily on λ and on the wall thickness. These cracks have been observed to close at about 20 °C with time and for the greatest part to heal in course of hardening, especially if the concrete gets moist cured. Over 100 °C no such "healing" is likely to occur.

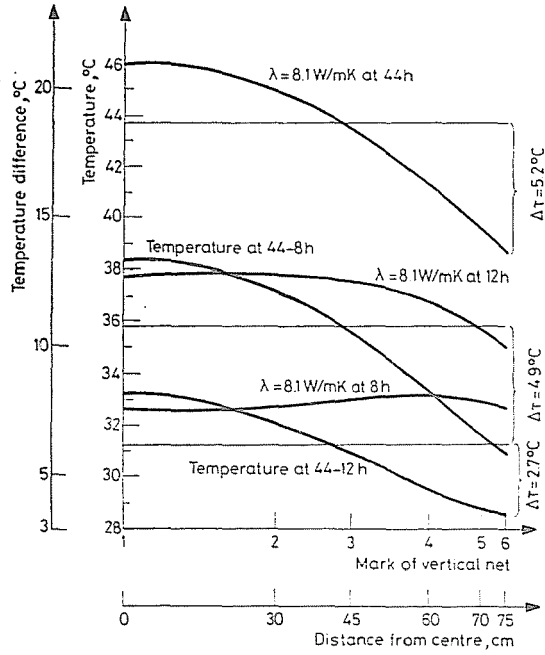


Fig. 18. Corrected temperature diagrams (example 11)

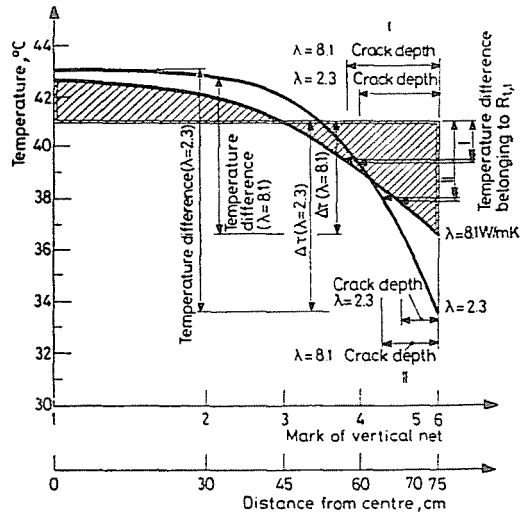


Fig. 19. Temperature distribution and crack depth vs. λ

Summary

Research was made on the dependence of the risk of crustal cracks on inner (time behaviour of concrete tensile strength, thermal conductivity and cement hydration heat release) and outer factors (shuttering, air temperature, insulation intensity, wind velocity, section-wise concreting).

Differential equation of thermal conductivity was solved by the method of elementary heat balance equations.

For the creep coefficient, to now not determined experimentally, Wischers suggested to reckon with a value $\varphi = 1$. Our suggestion is to subtract from the effective temperature diagram that one referring to the still plastic, stress-free concrete and starting from the resulting diagram for calculating the stresses. This range exempt from stresses still awaits to be checked by measurements.

References

1. ЛЫКОВ, А. В.: Теплообмен. Москва, 1972
2. КОРЧЕНОВА, Н. Н.—МАРОН, Ж. А.: Computational Mathematics. Mir, Moscow, 1975.
3. МИКНЕИЕВ, М. А.: Fundamentals of Heat Transfer. Mir, Moscow, 1968.
4. SCHIRMER, R.: VDI Beiheft Verfahrenstechnik, 1932.
5. БУДЫКО, М. И.: Тепловой баланс земной поверхности, Москва, 1956
6. Research on Causes and Prevention of the Cracking of the Concrete of Paks Nuclear Power Station I.* Research Report, Department of Building Materials, Technical University, Budapest, 1977.
7. WISCHERS, G.: Betontechnische und konstruktive Maßnahmen gegen Temperaturrisse in massigen Bauteilen. Beton Verlag, 1964.

Associate Prof. Dr. György BALÁZS, Head of Dept.	} H-1521, Budapest
Senior Assistant Dr. András TÓTH	
Research Officer István ZSIGOVICS	
János FEHÉR, Head of Section, ERÓTERV, V. Széchenyi rkp. 3. Budapest	

* In Hungarian